

Optical probe of strong correlations in LaNiO_3 thin films

M. K. Stewart,^{1,a)} Jian Liu,^{2,3} R. K. Smith,¹ B. C. Chapler,¹ C.-H. Yee,⁴ D. Meyers,² R. E. Baumbach,¹ M. B. Maple,¹ K. Haule,⁴ J. Chakhalian,² and D. N. Basov¹

¹*Department of Physics, University of California-San Diego, La Jolla, California 92093, USA*

²*Department of Physics, University of Arkansas, Fayetteville, Arkansas 72701, USA*

³*Advanced Light Source, Lawrence Berkeley National Laboratory, Berkeley, California 94720, USA*

⁴*Department of Physics and Astronomy, Rutgers University, Piscataway, New Jersey 08854-8019, USA*

(Received 26 January 2011; accepted 22 June 2011; published online 9 August 2011)

The optical properties of LaNiO_3 thin films are investigated over a wide energy and temperature range. Thin films of varying thickness were grown by pulsed laser deposition on LaAlO_3 and SrTiO_3 substrates. The optical conductivity data of the films reveal a number of interband transitions above 1 eV, which are in good agreement with band structure calculations. No well defined Drude peak is observed; however, in stark contrast with local-density approximation theory predicting a finite density of states at the Fermi energy. This experimental finding of a vanishing Drude spectral weight, compared to a finite electron kinetic energy obtained from band structure calculations, highlights the importance of strong electronic correlations in LaNiO_3 . © 2011 American Institute of Physics. [doi:10.1063/1.3614019]

I. INTRODUCTION

Transition metal oxides exhibit a wide array of interesting physical phenomena such as high temperature superconductivity, insulator-to-metal transitions, and half-metallic ferromagnetism.¹ Modern sample growth technologies offer an opportunity to control and tune these effects through heterostructuring.² At the interface between two oxides with different properties, the competing order parameters can dramatically modify the orbital, electronic, and magnetic structure of the bulk materials.³ Switching of superconductivity on and off, for instance, has been demonstrated at the interface between an oxide superconductor and an oxide ferroelectric.⁴ New properties not present in the constituent materials can also emerge at these interfaces. The formation of a metallic layer at the interface between the insulators LaAlO_3 and SrTiO_3 , for example, has already been demonstrated.⁵ Because of the ample choice of exotic properties offered by transition metal oxides for the growth of superlattices, experimental efforts will greatly benefit from the guidance of theoretical work. It is, therefore, of great importance that the constituent materials be thoroughly characterized experimentally and that their properties be well understood theoretically. This can be especially challenging, given that strong electronic correlations are often present in transition metal oxides.⁶

One of the most ambitious heterostructuring ideas yet is that of superconducting $\text{LaNiO}_3/\text{LaAlO}_3$ superlattices.^{7,8} Since the discovery of high-temperature superconductivity in the cuprates, the search for new superconducting materials with potentially higher transition temperatures has been at the vanguard of condensed matter physics research. LaNiO_3 (LNO) is in many ways similar to the cuprates, but with one important difference: it has one electron in two degenerate, three-dimensional e_g orbitals. The lack of orbital degeneracy

and the quasi two-dimensionality of the e_g electrons are well established attributes of superconductivity in the cuprates. Modifying the orbital structure of LNO through layered heterostructuring, and successfully inducing superconductivity in this non-superconducting material, would be a major breakthrough. Because of this, and given our limited understanding of LNO thus far, a detailed optical study of this oxide promises to be of great use.

In the bulk, LNO is a paramagnetic metal with a rhombohedrally distorted perovskite crystal structure.⁹ Resistivity, susceptibility, and heat capacity data reported for powder

LNO are suggestive of strong correlations in this system.¹⁰ Unlike other rare earth nickelates, LNO does not exhibit a temperature controlled metal-insulator transition, but an antiferromagnetic insulating state has been reported in oxygen deficient LaNiO_{3-x} .^{11,12} In this work, we show that LNO is a correlated electron system, as evidenced by an experimental Drude spectral weight that is strongly suppressed compared to that predicted by band structure calculations. The optical data presented here cannot be fully described by available theoretical models of LNO. We propose that a better theoretical understanding of LNO is essential in order to fully explore the possibilities and limitations of $\text{LaNiO}_3/\text{LaAlO}_3$ superlattices.

II. METHODS

Bulk synthesis of LNO has been a challenging issue, with available single crystals limited to the micron size. Thin film deposition, on the other hand, is largely possible because of the epitaxial stabilization.¹³ Thus, by pulsed laser deposition, we grew preferentially (001)-oriented LNO films on LaAlO_3 (LAO) and SrTiO_3 (STO) single crystal substrates. A KrF excimer laser ($\lambda = 248$ nm) was used to ablate a stoichiometry LNO target under 100 mTorr oxygen partial pressure. The temperature during the growth was kept at 700 °C and cooled to 600 °C after deposition, where annealing was

^{a)}Electronic mail: mstewart@physics.ucsd.edu.

performed under 1 atm of oxygen for one hour. To probe the bulk behavior of LNO, the film thicknesses are 100 nm and 200 nm, which are sufficiently larger than the critical thickness; therefore, relaxing the structure and minimizing strain-induced distortions. The effect of strain is further isolated by comparing films subjected to opposite lattice mismatch from LAO (−1.3%) and STO (+1.8%) substrates. Representative $\theta - 2\theta$ x-ray diffraction data for the 200 nm film on STO are shown in Fig. 1. The scans reveal all (001) reflections corresponding to a (001)-oriented perovskite structure. A (110) peak commonly found in thick films is also evident. The relative intensities of the (110) and (002) peaks indicate that the (110) phase makes up much less than 0.8% of the film.¹⁴ The *c*-axis parameters are 3.84 Å and 3.86 Å on STO and LAO, respectively. While the former is the same as the bulk,⁹ indicating complete relaxation from the large tensile strain, the latter is slightly bigger likely due to residual strain from the relatively smaller lattice mismatch.

Optical studies of both the films and the bare substrates were carried out using reflectance in the range from 50 to 700 cm^{-1} and variable angle spectroscopic ellipsometry (VASE) in the range from 700 to 48 000 cm^{-1} . Near-normal incidence reflectance measurements were performed in a Michelson interferometer (Bruker 66vs). Reflectance of the sample was first measured relative to a gold reference mirror and then normalized by the reflectance of the gold coated sample.¹⁵ Ellipsometry measurements were performed with two commercial Woollam ellipsometers. The range from 700 to 4500 cm^{-1} was investigated with an IR-VASE model based on a Bruker 66vs. For the range between 5000 and 48 000 cm^{-1} , we used a VASE model based on a grating monochromator. Both ellipsometers are equipped with home-built UHV chambers to allow low temperature measurements.¹⁶ All the samples were characterized over the entire frequency range at room temperature and in some cases at low temperatures down to 20 K. Ellipsometry measurements were performed at incidence angles of 60° and 75°. At each angle, the polarization state of the reflected light was measured in the form of two parameters, Ψ and Δ , which are related to the Fresnel reflection coefficients for *p*- and *s*-polarized light (R_p and R_s) through the equation

$$\frac{R_p}{R_s} = \tan(\Psi)e^{i\Delta}.$$

In order to obtain the optical constants from the raw reflectance and ellipsometry data, a model was created using Kramers-Kronig consistent Lorentz oscillators to describe the complex dielectric function of the sample. The parameters in the model were then fitted to the experimental data using regression analysis.¹⁷ In the case of the LNO films, the model consisted of two layers: a substrate characterized by the optical constants previously determined for either LAO or STO, and a thin film layer from which the optical constants of the film alone were obtained. Figure 2 shows the raw reflectance and ellipsometry data plotted with the model fit for the 100 nm film on STO. The STO substrate phonons at 175 cm^{-1} and 483 cm^{-1} are evident in the reflectance data and have been accounted for in our model.

Local-density approximation (LDA) band structure was computed within the full-potential linearized augmented plane wave (FP-LAPW) scheme¹⁸ using room temperature bulk LNO structural parameters.⁹ The calculations were performed on a 9 × 9 × 9 *k*-space grid with the $R_x K_{\text{max}}$ parameter controlling the cut-off for augmented plane waves set to 9.0, and converged to 0.1 mRy in energy and 0.0005 in charge distance.

III. RESULTS AND DISCUSSION

Transport data in Fig. 3 show metallic behavior and reveal the resistivity of the films to be on the order of 1 m Ω cm. This value is in good agreement with previously reported transport data for similar films¹⁹ and bulk LNO.^{10,20} The resistivity of our films is higher than that of ultrathin films of LNO,^{21,22} which we attribute to the difference in thickness. It is known that thickness and strain can strongly influence the transport properties of LNO thin films.²² The 100–200 nm films used in this work are expected to be essentially strain-free while ultrathin films of thickness 20 nm or less contain at least a significant fraction that is subject to epitaxial strain due to the substrate. The resistivity data in Fig. 3 show an upturn

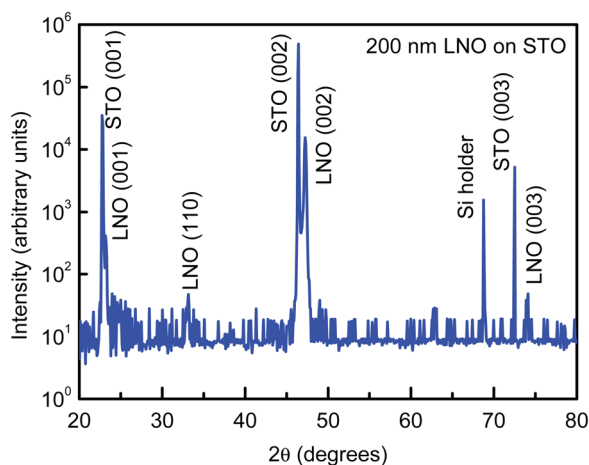


FIG. 1. (Color online) $\theta - 2\theta$ x-ray scan for the 200 nm film on STO.

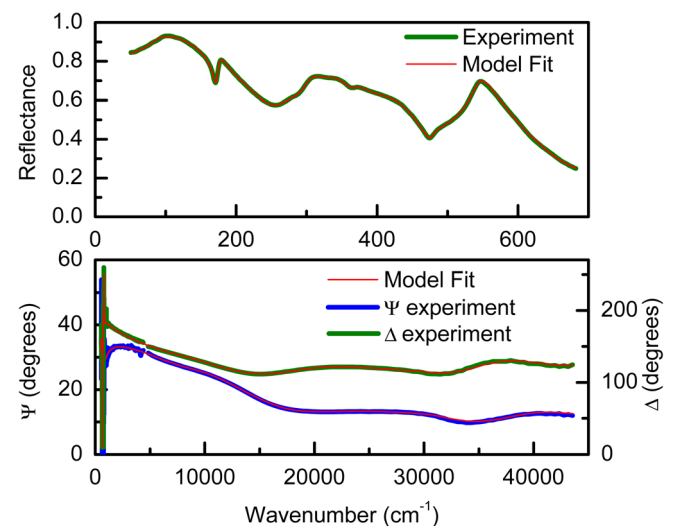


FIG. 2. (Color online) Raw reflectance (top panel) and 60° ellipsometry (bottom panel) data for the 100 nm film on STO plotted with the fit from the model (thin red line).

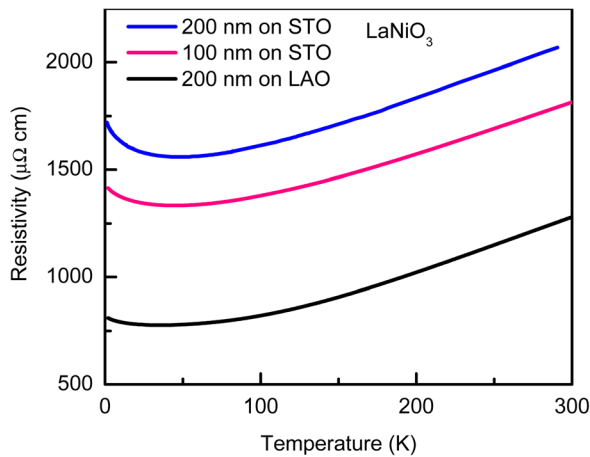


FIG. 3. (Color online) DC resistivity of the LNO films over a wide temperature range.

at low temperature. The same behavior is reported in Ref. 19 and is attributed to quantum corrections to the conductivity due to weak localization and renormalization of electron-electron interactions. A similar low temperature upturn in the resistivity has been observed in other correlated oxides.^{23–25}

To gain insight into the electronic band structure of LNO, it is useful to look at the optical conductivity, which is related to the complex dielectric function through the equation $\sigma(\omega) = i\omega[1 - \epsilon(\omega)]/4\pi$. Figure 4 shows the real, dissipative part of the optical conductivity at room temperature. In the high energy region, above 1 eV, the main features of the optical conductivity, which we have labeled B-E, look similar for all the films. A more noticeable variation in the spectra is evident in the mid-IR region, presumably due to the effects of strain. While all samples show a peak in this region (A in Fig. 4), the magnitude and shape is different for each film. In the far-IR range (note the change in scale), we see a broad peak centered at 300 cm^{-1} . In stark contrast with theoretical predictions, no well defined Drude peak is observed, indicative of very strong electronic correlations. Below we discuss in detail the data in these three regions. The similarity of the

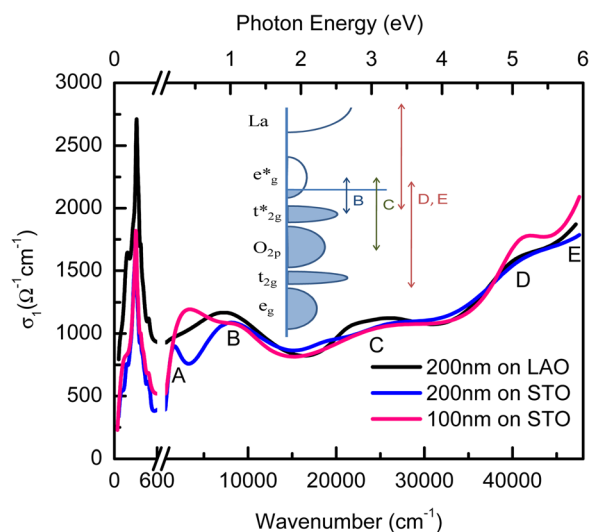


FIG. 4. (Color online) Real part of the optical conductivity of three different LNO films at room temperature. Note the change in scale at 600 cm^{-1} . Inset: rough sketch of the LNO density of states and interband transitions.

100 nm and 200 nm films on STO seen in Fig. 4, especially in the far-IR region, shows that the small fraction of secondary phases that may develop with increasing thickness do not significantly affect the optical conductivity of the films. Additionally, the similarity of the films on STO and LAO indicates that our data indeed reflect the properties of strain-free LNO.

The high energy optical conductivity we have acquired is consistent with earlier work on LNO ceramic samples.^{26,27} In Fig. 5, we plot the calculated LDA partial density of states, which is in good agreement with previous band structure calculations.^{28–30} LNO has a $t_{2g}^6 e_g^1$ electronic configuration, with the antibonding e_g states crossing the Fermi level. The inset in Fig. 5 shows that the optical conductivity obtained from LDA calculations is in qualitative agreement with our experimental data. Based on the data in Fig. 5 and using transition decomposition analysis of the LDA optical conductivity, we attempt to assign features B-D in Fig. 4 to specific interband transitions (see inset in Fig. 4). We suggest that B corresponds to transitions from the Ni t_{2g}^* and e_g^* levels to the Ni e_g^* orbitals. C could be due to transitions from the O $2p$ to the e_g^* orbitals. D and E may be the result of transitions from t_{2g}^* to the La $4f$ and $5d$ levels and from the bonding Ni e_g and t_{2g} orbitals to the e_g^* orbitals. Low temperature optical conductivity in this range is shown in the inset of Fig. 6. All of the features remain unchanged down to 20 K. A small reduction of up to 5% in the optical conductivity is evident between 1.5 and 4 eV.

Based on LDA calculations, feature A in the mid-IR region appears to be too low in energy to be an interband transition. However, given the failure of this model to accurately describe our low frequency data, it is possible that the e_g^* band is, in reality, significantly different from that obtained by these calculations. In this scenario, it cannot be ruled out that this peak is indeed associated with an interband transition.

Alternatively, feature A could be a sign of some kind of electron localization. It is known that localization phenomena can give rise to a shift of the Drude peak to finite frequencies,

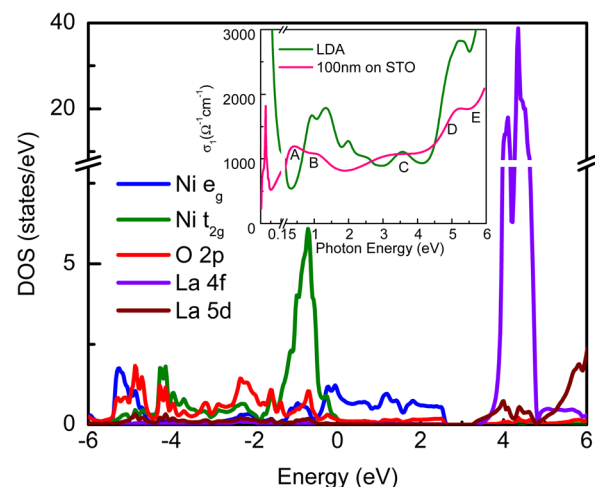


FIG. 5. (Color online) Partial LNO density of states obtained from LDA theory. Inset: comparison of the optical conductivity obtained experimentally for the 200 nm film of LNO on STO and that obtained from LDA calculations. The Drude peak produced by LDA theory is not present in the experimental data.

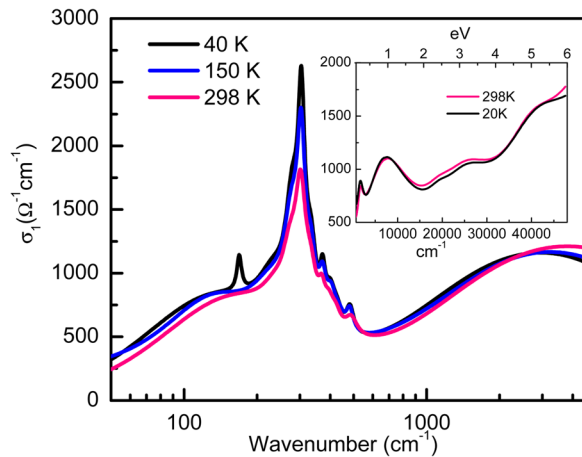


FIG. 6. (Color online) Low temperature optical conductivity of the 100 nm thick film on STO in the far-IR and mid-IR regions. Inset: optical conductivity of the 200 nm film on STO up to 6 eV at 298 and 20 K.

due to the need of the electrons to overcome an energy barrier.³¹ We note that the peak does seem to be centered at an unusually high energy compared to other materials where localization of electrons is present.^{32,33} Polaronic transport can also result in this type mid-IR absorption. Figure 6 shows low temperature infrared data for the 100 nm film on STO. Virtually no temperature dependence of this feature is observed down to 40 K. This behavior allows us to rule out the presence of small polarons, which would require a strong temperature dependence of the mid-IR absorption.³⁴ Large polaron absorption spectra, on the other hand, are expected to be temperature independent and asymmetric,³⁵ in agreement with our data. The peak position near 0.3 eV is also consistent with large polarons, as it is below the 0.7 eV cutoff predicted by Fröhlich coupling for transition metal oxides.³¹ It has also been suggested that this type of absorption could be due to incoherent motion of carriers coupled to the spin degree of freedom.²⁷ However, the lack of temperature dependence in our data makes this an unlikely scenario.

We now focus our attention on the far-IR part of the spectra in Fig. 4. Optical measurements are ideal for probing the kinetic energy of electrons, given that this quantity is proportional to the area under the Drude part of the optical conductivity, $K_{exp} \propto \int_0^{\infty} \sigma_1(\omega) d\omega$.³⁶ Comparison of the experimental electron kinetic energy to that obtained from band structure calculations, K_{band} , provides a means for classifying materials according to the strength of the electronic correlations in the system.^{37,38} The ratio K_{exp}/K_{band} is expected to be close to unity for itinerant electron systems and will become suppressed as strong interactions come into play, which are not included in K_{band} . Band structure calculations for LNO predict a finite density of states at the Fermi level and a plasma frequency $\omega_p = 3.7$ eV. Data in Fig. 4, however, show no obvious sign of a Drude contribution to the optical conductivity. The plasma frequency obtained by integrating $\sigma_1(\omega)$ up to 1500 cm^{-1} is 1 eV for the film on LAO and 0.8 eV for the films on STO. This results in $K_{exp}/K_{band} \approx 0.05 - 0.07$, which is quite low, even compared to other correlated metals.³⁸ In this context, our data present robust evidence of very strong electronic correlations in LNO. These values are also

low compared to those of ultrathin strained LNO films which, while still very strongly correlated, do exhibit a Drude peak.³⁹ This suggests that strain affects the electronic properties of LNO.

In contrast with other lanthanide rare earth nickelates,^{40,41} the strength of correlations in LNO does not appear to be tuned by temperature. The low temperature data in Fig. 6 show no significant temperature dependence, except for the peak at 300 cm^{-1} , which we discuss below. Low temperature far-IR data have also been obtained for the film on LAO but are not shown here, as they exhibit the same trend as the data in Fig. 6. We note that, even in the realm of strongly correlated systems, the low energy optical conductivity spectra we have obtained is unusual. Correlated metals typically show coherent (Drude) and incoherent contributions of similar strength. In the case of LNO, the incoherent part of the optical conductivity (feature A) is much stronger than the coherent one.

We now discuss the strong far-IR resonance shown in Figs. 4 and 6. According to group theory, three infrared-active phonon modes are expected in this range for a cubic perovskite. The broad peak centered at 300 cm^{-1} is composed of much more than three oscillators. One possibility is that the modes are split and broadened due to the rhombohedral distortion of the LNO lattice. At 40 K, the strength of the main peak is increased by about 20% and a small peak is resolved at 170 cm^{-1} (Fig. 6). This, along with some sharpening of the spectra at low temperature, is suggestive of absorption due to phonons. The effective ionic charge obtained from this resonance by means of the equation

$$\int \sigma_1(\omega) d\omega = \frac{\pi n Z^2}{2m^*},$$

is $Z = 2.5$. While this value is somewhat high, it is not outside the range of known effective ionic charges in oxides.^{27,42} In nickelates, $Z = 1.9$ has been obtained for $\text{La}_2\text{NiO}_{4+\delta}$.⁴³ As seen in Fig. 4, no thickness dependence of this feature is observed, with the 100 nm and 200 nm films on STO showing almost identical far-IR spectra. The film on LAO shows optical conductivity about 50% higher than the films on STO, consistent with resistivity data. The shape of the resonance, however, is remarkably similar even though LAO has a rhombohedral perovskite crystal structure and STO is a cubic perovskite.

A recent x-ray photoemission study of LNO has found a dispersive e_g band crossing the Fermi energy, in apparent disagreement with our data.⁴⁴ A similar discrepancy between angle resolved photoemission spectroscopy (ARPES) and infrared optical data has been reported for layered manganites and can be explained by the presence of a pseudogap at the Fermi energy.^{45,46} It is also important to note that LNO is a polar material in which electronic reconstruction at the surface is a likely possibility.⁴⁷ While the results of Ref. 44 show a 3D Fermi surface with k_z band dispersion, the probing thickness of ARPES is still very small compared to infrared probes. It cannot be ruled out that these data are a more accurate description of the electronic structure of LNO in the vicinity of a surface or interface than of bulk LNO.

IV. CONCLUSIONS

We have obtained optical conductivity of various LNO thin films over a wide temperature and energy range. Above 1 eV, our data show several interband transition in good agreement with band structure calculations. At lower frequencies, however, significant discrepancies with theory are evident. Despite band theory predictions of a finite density of states at the Fermi level, no Drude peak is present in our data. We claim that this is evidence of strong correlations in LNO, which must be taken into account by theoretical models used in the design of oxide heterostructures. We have shown that the strength of the electronic correlations is not controlled by temperature.

ACKNOWLEDGMENTS

The authors thank A. J. Millis, S. J. Moon, and G. Sawatzky for useful discussion. Work at UCSD was supported by DOE-BES. J.C. was supported by DOD-ARO under Grant No. 0402-17291 and NSF Grant No. DMR-0747808. M.B.M. was supported by DOE under Grant No. DE FG02-04ER46105.

- ¹J. B. Goodenough, *Rep. Prog. Phys.* **67**, 1915 (2004).
- ²T. Venkatesan, X. D. Wu, A. Inam, and J. B. Wachtman, *Appl. Phys. Lett.* **52**, 1193 (1988).
- ³J. W. Reiner, F. J. Walker, and C. H. Ahn, *Science* **323**, 1018 (2009).
- ⁴K. S. Takahashi, M. Gabay, D. Jaccard, K. Shibuya, T. Ohnishi, M. Lippmaa, and J. M. Triscone, *Nature* **441**, 195 (2006).
- ⁵A. Ohtomo and H. Y. Hwang, *Nature* **427**, 423 (2004).
- ⁶Y. Tokura, *Phys. Today* **56**(7), 50 (2003).
- ⁷J. Chaloupka and G. Khaliullin, *Phys. Rev. Lett.* **100**, 016404 (2008).
- ⁸P. Hansmann, X. P. Yang, A. Toschi, G. Khaliullin, O. K. Andersen, and K. Held, *Phys. Rev. Lett.* **103**, 016401 (2009).
- ⁹J. L. Garcia-Munoz, J. Rodriguez-Carvajal, P. Lacorre, and J. B. Torrance, *Phys. Rev. B* **46**, 4414 (1992).
- ¹⁰K. Sreedhar, J. M. Honig, M. Darwin, M. McElfresh, P. M. Shand, J. Xu, B. C. Crooker, and J. Spalek, *Phys. Rev. B* **46**, 6382 (1992).
- ¹¹R. D. Sanchez, M. T. Causa, A. Caneiro, A. Butera, M. Vallet-Regi, M. J. Sayagues, J. Gonzalez-Calbet, F. Garcia-Sanz, and J. Rivas, *Phys. Rev. B* **54**, 16574 (1996).
- ¹²K. Horiba, R. Eguchi, M. Taguchi, A. Chainani, A. Kikkawa, Y. Senba, H. Ohashi, and S. Shin, *Phys. Rev. B* **76**, 155104 (2007).
- ¹³A. R. Kaul, O. Yu Gorbenco, and A. A. Kamenev, *Russ. Chem. Rev.* **73**, 861 (2004).
- ¹⁴B. Berini, N. Keller, Y. Dumont, E. Popova, W. Noun, M. Guyot, J. Vigneron, A. Etcheberry, N. Franco, and R. M. C. da Silva, *Phys. Rev. B* **76**, 205417 (2007).
- ¹⁵C. C. Homes, M. Reedyk, D. A. Cradles, and T. Timusk, *Appl. Opt.* **32**, 2976 (1993).
- ¹⁶K. S. Burch, J. Stephens, R. K. Kawakami, D. D. Awschalom, and D. N. Basov, *Phys. Rev. B* **70**, 205208 (2004); M. K. Stewart, K. B. Chetry, B. Chapler, M. M. Qazilbash, A. A. Schafgans, A. Gupta, T. E. Tiwald, and D. N. Basov, *Phys. Rev. B* **79**, 144414 (2009); M. K. Stewart, C.-H. Yee, J. Liu, M. Kareev, R. K. Smith, B. C. Chapler, M. Varela, P. J. Ryan, K. Haule, J. Chakhalian, and D. N. Basov, *Phys. Rev. B* **83**, 075125 (2011).
- ¹⁷A. B. Kuzmenko, *Rev. Sci. Instr.* **76**, 083108 (2005).
- ¹⁸P. Blaha, K. Schwartz, G. K. H. Madsen, D. Kvasnicka, and J. Luitz, *An Augmented Plane Wave + Local Orbitals Program for Calculating Crystal Properties* (Karlheinz Schwarz, Techn. Universitat, Wien, 2001).
- ¹⁹Y. Kumar, R. J. Choudhary, A. P. Singh, G. Anjum, and R. Kumar, *J. Appl. Phys.* **108**, 083706 (2010).
- ²⁰K. P. Rajeev, G. V. Shivashankar, and A. K. Raychaudhuri, *Solid State Commun.* **79**, 591 (1991).
- ²¹K. Tsubouchi, I. Ohkubo, H. Kumigashira, Y. Matsumoto, T. Ohnishi, M. Lippmaa, H. Koinuma, and M. Oshima, *Appl. Phys. Lett.* **92**, 262109 (2008).
- ²²J. Son, P. Moetakef, J. M. LeBeau, D. Ouellette, L. Balents, S. J. Allen, and S. Stemmer, *Appl. Phys. Lett.* **96**, 062114 (2010).
- ²³Y. Ando, G. S. Boebinger, A. Passner, T. Kimura, and K. Kishio, *Phys. Rev. Lett.* **75**, 4662 (1995).
- ²⁴Y. Ando, G. S. Boebinger, A. Passner, N. L. Wang, C. Geibel, and F. Steglich, *Phys. Rev. Lett.* **77**, 2065 (1996).
- ²⁵G. Herranz, B. Martinez, J. Fontcuberta, F. Sanchez, C. Ferrater, M. V. Garcia-Cuenca, and M. Varela, *Phys. Rev. B* **67**, 174423 (2003).
- ²⁶T. Arima, Y. Tokura, and J. B. Torrance, *Phys. Rev. B* **48**, 17006 (1993).
- ²⁷T. H. Arima and Y. Tokura, *J. Phys. Soc. Jpn.* **64**, 2488 (1995).
- ²⁸D. D. Sarma, N. Shanthi, and P. Mahadevan, *J. Phys. Cond. Matt.* **6**, 10467 (1994).
- ²⁹I. Solovyev, N. Hamada, and K. Terakura, *Phys. Rev. B* **53**, 7158 (1996).
- ³⁰Y. Nohara, S. Yamamoto, and T. Fujiwara, *Phys. Rev. B* **79**, 195110 (2009).
- ³¹D. N. Basov, R. D. Averitt, D. van der Marel, M. Dressel, and K. Haule, *Rev. Mod. Phys.* **83**, 471 (2011).
- ³²D. N. Basov, A. V. Puchkov, R. A. Hughes, T. Strach, J. Preston, T. Timusk, D. A. Bonn, R. Liang, and W. N. Hardy, *Phys. Rev. B* **49**, 12165 (1994).
- ³³D. N. Basov, B. Dabrowski, and T. Timusk, *Phys. Rev. Lett.* **81**, 2132 (1998).
- ³⁴H. G. Reik and D. Heese, *J. Phys. Chem. Solids* **28**, 581 (1967).
- ³⁵D. Emin, *Phys. Rev. B* **48**, 13691 (1993).
- ³⁶A. J. Millis, A. Zimmers, R. P. S. M. Lobo, N. Bontemps, and C. C. Homes, *Phys. Rev. B* **72**, 224517 (2005).
- ³⁷A. J. Millis, in *Strong Interactions in Low Dimensions*, edited by D. Baeriswyl and L. Degiorgi (Kluwer Academic, Dordrecht, 2004).
- ³⁸M. M. Qazilbash, J. J. Hamlin, R. E. Baumbach, L. J. Zhang, D. J. Singh, M. B. Maple, and D. N. Basov, *Nat. Phys.* **5**, 647 (2009); D. N. Basov and A. V. Chubukov, *Nat. Phys.* **7**, 272 (2011).
- ³⁹D. G. Ouellette, S. B. Lee, J. Son, S. Stemmer, L. Balents, A. J. Millis, and S. J. Allen, *Phys. Rev. B* **82**, 165112 (2010).
- ⁴⁰T. Katsufuji, Y. Okimoto, T. Arima, Y. Tokura, and J. B. Torrance, *Phys. Rev. B* **51**, 4830 (1995).
- ⁴¹M. A. Mroginiski, N. E. Massa, H. Salva, J. A. Alonso, and M. J. Martinez-Lope, *Phys. Rev. B* **60**, 5304 (1999).
- ⁴²F. Gervais, *Mat. Sci. Eng. R* **39**, 29 (2002).
- ⁴³N. Poirot, V. T. Phuoc, G. Gruener, and F. Gervais, *Solid State Sci.* **7**, 1157 (2005).
- ⁴⁴R. Eguchi, A. Chainani, M. Taguchi, M. Matsunami, Y. Ishida, K. Horiba, Y. Senba, H. Ohashi, and S. Shin, *Phys. Rev. B* **79**, 115122 (2009).
- ⁴⁵Y. D. Chuang, A. D. Gromko, D. S. Dessau, T. Kimura, and Y. Tokura, *Science* **292**, 1509 (2001).
- ⁴⁶T. Ishikawa, T. Kimura, T. Katsufuji, and Y. Tokura, *Phys. Rev. B* **57**, R8079 (1998).
- ⁴⁷P. W. Tasker, *J. Phys. C* **12**, 4977 (1979).